metals

MDPI

Article

Effect of Calefaction and Stress Relaxation on Grain Boundaries/Textures of Cu–Cr–Ni Alloy

Haitao Liu [1,2,*], Guojie Wang [1], Kexing Song [1,3], Yunxiao Hua [1], Yong Liu [1] and Tao Huang [1,2]

[1] School of Materials Science and Engineering, Henan University of Science and Technology, Luoyang 471023, China; 13346945723@163.com (G.W.); kxsong@haust.edu.cn (K.S.); huayunxiao@163.com (Y.H.); liuyong209@haust.edu.cn (Y.L.); huangtao@haust.edu.cn (T.H.)
[2] Provincial and Ministerial Co-Construction of Collaborative Innovation Center for Non-Ferrous Metal New Materials and Advanced Processing Technology, Luoyang 471023, China
[3] Henan Academy of Sciences, Zhengzhou 450002, China
* Correspondence: htliu@haust.edu.cn

Abstract: The Cu–Cr–Ni alloy is a key material for the manufacturing of connectors, which requires excellent resistance to stress relaxation. However, the inherent correlation among microstructure, texture, and properties is still unclear. In this study, we investigated the influence of calefaction and stress relaxation on the grain boundaries (GBs), textures, and properties of the Cu–Cr–Ni alloy. The results showed that calefaction and stress relaxation had opposite effects on GBs and textures. Calefaction led to a decrease in the proportion of low-angle grain boundaries (LAGBs), an increase in the Schmidt factor (SF) value of the grains, and a transition of texture from <111> to <113>. The grains with higher SF values were more susceptible to plastic deformation, which deteriorated the stress relaxation resistance. By comparison, stress relaxation led to an increase in the proportion of LAGBs, a decrease in SF values of the grains, and a transition of texture from <113> to <111> and <001>. After stress relaxation, the variation trends of the GBs and textures were consistent with those of other plastic deformations, indicating that stress relaxation can be verified by the variations in GBs and textures. Our findings provide a theoretical basis for improvements in stress relaxation resistance of the Cu-based alloys used in connector industry.

Keywords: Cu–Cr–Ni alloy; calefaction; stress relaxation; grain boundaries; texture

check for updates

Citation: Liu, H.; Wang, G.; Song, K.; Hua, Y.; Liu, Y.; Huang, T. Effect of Calefaction and Stress Relaxation on Grain Boundaries/Textures of Cu–Cr–Ni Alloy. *Metals* **2024**, *14*, 837. https://doi.org/10.3390/met14070837

Academic Editor: Marcello Cabibbo

Received: 1 June 2024
Revised: 1 July 2024
Accepted: 15 July 2024
Published: 22 July 2024

Copyright: © 2024 by the authors. Licensee MDPI, Basel, Switzerland. This article is an open access article distributed under the terms and conditions of the Creative Commons Attribution (CC BY) license (https://creativecommons.org/licenses/by/4.0/).

1. Introduction

Stress relaxation resistance is the primary index for connectors [1,2]. Most of the terminal materials are made of copper (Cu) alloys. However, steel- or nickel-based alloys have been adopted under special conditions (high-temperature, wear-resistant conditions). With the development and application of connectors, higher requirements have been put forward for their high-current miniaturization and high-temperature performance. Therefore, terminal materials need to have high electrical conductivity, excellent formability, and high resistance to thermal stress relaxation. Cu and its alloys greatly meet the needs of electrical conductivity and formability, but their heat-resistant performances are not outstanding [3,4]. In general, Cu alloys are less resistant to thermal stress relaxation. Exploring the effect of calefaction on stress relaxation resistance is a hot research topic regarding the application of Cu alloys in connectors.

Yang et al. [5] investigated the effect of temperature on the stress relaxation resistance of coarse-grained, nano-grained, and nano-twinned Cu. It was demonstrated by high resolution transmission electron microscope (HRTEM) and molecular dynamics (MD) that stress relaxation at high temperatures was related to dislocation-mediated plastic deformation. The higher temperature contributed to faster stress relaxation. Lyu et al. [6] investigated the effect of stress and temperature on the stress relaxation of an Al–Mg–Zn alloy. The results showed that a high temperature was favorable for dislocation movement,

which accelerated stress relaxation. Stress relaxation tests were performed on Ti–6Al–4V by Peng et al. [7]. The results showed that temperature enhanced the ability of atomic diffusion and dislocation movement. The temperature shortened the time to reach the second stage of stress relaxation. In the studies of various scholars, experimental results have shown that high temperatures can deteriorate the stress relaxation resistance of materials [8–10]. The effect of calefaction on stress relaxation has mostly been discussed by the dislocation theory. There is no doubt that calefaction can also significantly influence the texture [11–15]. However, the effect of calefaction on stress relaxation has rarely been reported on from the perspective of texture.

Texture has a close correlation with performance. For example, the quality of a deep-drawing sheet is directly related to the types of texture, and the ideal textures are {111} <112> and {111} <110> [16]. The texture also closely correlates with other properties. Chen et al. [17] performed hot rolling, followed by cold rolling, on aluminum foil and discovered that the yield strength was reduced due to the increase in soft orientation. Yang [18] performed a cold drawing test on low-oxygen Cu wires. The plastic deformation was dominated by a plane slip and formed the <111> texture at low tensile strain. The <111> and <100> textures were interlaced in distribution at high tensile strain. The experimental results showed that the yield strength of the material was influenced by textures. Many scholars have since investigated the relationship between textures and properties, such as stretch, compression, and electrical conductivity, proving that textures are correlated with material properties [19–25]. However, the relationship between textures and stress relaxation remains unclear.

Statistically, it was found that the research on stress relaxation of Cu alloys has mainly been focused on precipitation strengthening and solid solution strengthening [9,26–29]. The effect of textures on material properties has mainly been focused on conventional mechanical properties [16–25]. However, the study of the relationship between textures and stress relaxation is rare. Stress relaxation may be exacerbated by calefaction. The effect of calefaction on stress relaxation from a standpoint of texture has also been rarely elaborated on. Therefore, the evolution of the texture due to calefaction or stress relaxation and the essence of stress relaxation were investigated in the present study.

2. Material and Methods

A Cu–Cr–Ni alloy ingot was melted in a vacuum induction furnace. Table 1 shows the chemical compositions of the alloy. The ingot was annealed at 980 °C for 2.5 h. Subsequently, the ingot, with a thickness of 16 mm, was subjected to hot extrusion by 4 passes. After hot rolling, the thickness of sheet was 5.3 mm and the total reduction was 67%. Water cooling was carried out immediately to maintain the solid solution microstructure. Then, the sheet was subjected to cold rolling with large deformation, and a sheet with a 0.9 mm thickness was finally obtained, with a total deformation of 83%, by 5 passes. The sheet-forming process is shown in Figure 1.

Table 1. The elementary analysis of the Cu–Cr–Ni alloy (mass fraction, wt.%) [30].

Alloy	Cr	Ni	Ti	Fe	Si	Zr	Cu
Cu-Cr-Ni	0.27	0.19	0.058	0.034	0.028	0.0036	Bal.

The cold-rolled specimens were subjected to an aging treatment at 450 °C for 1 h in the vacuum tube furnace (STGK-100-12, Sante Furance Corporation, Luoyang, China). The samples for the tensile and stress relaxation tests were prepared by electrical discharge machining from the aged sheets; the dimensions followed GB/T 34505-2017 [31] with a gauge length of 60 mm. The tensile rate was 0.75 mm/min. $R_{p0.2}$ was calculated from the tensile data and taken as the yield strength. The uniaxial tensile test method was used for the stress relaxation test. The initial stress of the stress relaxation test was half of the yield strength, and the test environment was 194.7 °C for 24 h. For the macro- and microscopic investigations, optical microscopy (OM, OLYMPUSPMG3, Olympus Corporation, Tokyo,

Japan) was performed on the mechanically ground and polished surfaces of the aged specimens. The TEM samples were prepared from the aged state. Cylinders of 3 mm in diameter were spark eroded and cut into thin discs of 500 µm with a diamond saw. These discs were ground down to 100 µm using SiC paper. Electron transparency was achieved by twin-jet polishing in the MTP-1A system with a voltage of 20 V at 10 °C. The electrolyte consisted of phosphoric acid, ethanol, and deionized water, with a volume ratio of 1:1:1. The TEM investigations were carried out on FEI Talos F200X (FEI Corporation, Waltham, MA, USA) operated at an accelerating voltage of 200 kV. The selected area electron diffraction (SAD) was performed to resolve the exact crystal structure of the Cr precipitates. Electron backscatter diffraction (EBSD) was performed on OXFORD NordlysMax3 (Oxford Instruments, Oxford, UK) to investigate the texture under different treatment processes. The major texture components were counted with the deviation angle of ±15°. The data processing was carried out in CHANNEL 5 software.

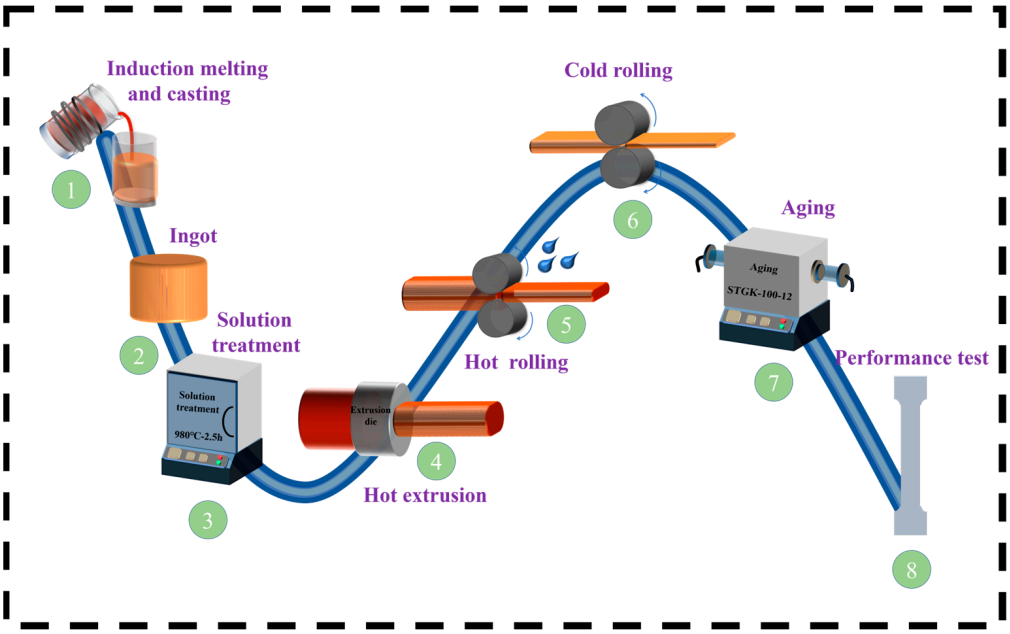


Figure 1. The material forming process.

3. Results and Discussion

3.1. Properties and Microstructure

The tensile strength of the Cu–Cr–Ni alloy was 480 MPa (Figure 2a). The $R_{p0.2}$ of the alloy was 440 MPa, which was calculated from the tensile curve. The stress relaxation curve is shown in Figure 2b. After stress relaxation, the percentage of residual stress was 93.1%. As can be seen from Figure 2b, the stress relaxation curve was divided into two stages. In the first stage, the stress decreased rapidly, and in the second stage, it gradually leveled off.

The microstructure of the aged specimen was observed, including metallography, precipitation, and dislocations. Figure 3 shows the metallography of the aged specimen, and it can be seen that the grains are in a broken state. The grains appear as long strips rather than isometric crystal. Most of the grains have a length of greater than 150 µm and a width of less than 70 µm. The average ratio of the grain length to its transverse size L/D was 2.3. No obvious precipitation was found in the metallographic microstructure.

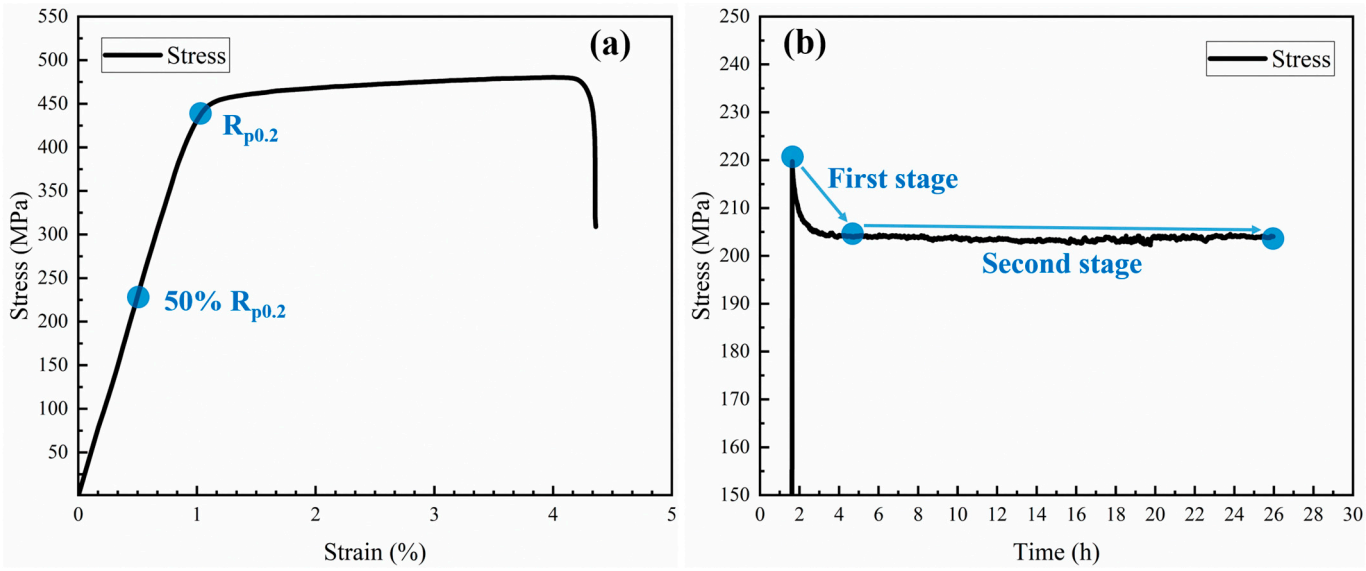


Figure 2. (**a**) Tensile curve at room temperature and (**b**) stress relaxation curve at 194.7 for 24 h.

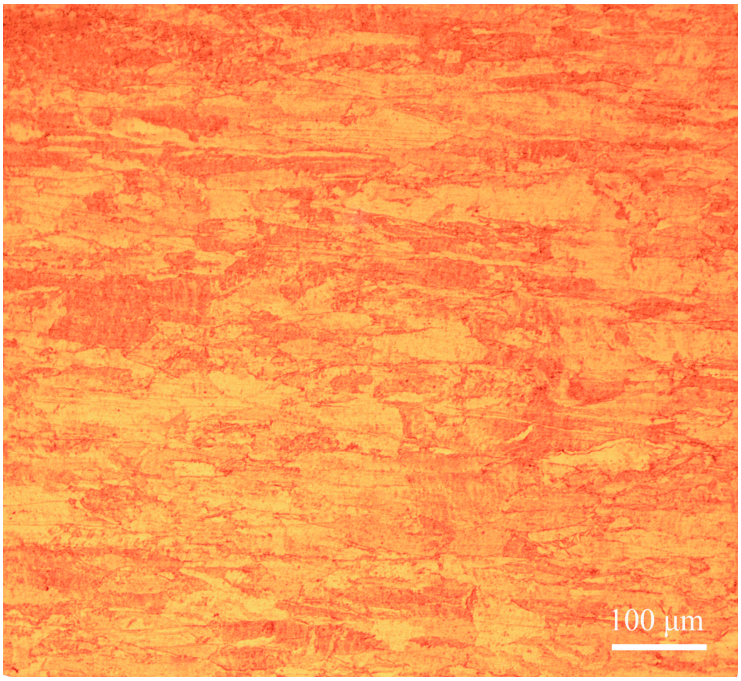


Figure 3. Metallography of Cu–Cr–Ni alloy in aging state.

The results of the TEM investigations of the precipitates in the aged Cu–Cr–Ni alloy were analyzed and are shown in Figure 4. In Figure 4a, the precipitates are oval or round. Figure 4b,c show the EDS point analyses of precipitates 1 and 2, respectively. The results indicate that both of them are Cr-rich phases. Figure 4d shows a randomly selected precipitate in a Cu–Cr–Ni alloy. The SAD and map scanning of the representative precipitation show that it is an elemental Cr phase with bcc structure, as presented in Figure 4e–g.

Precipitation and textures are relational, and precipitation can affect textures and properties under the influence of tension or calefaction [32,33]. In the follow-up work, precipitation was considered as a process variable in the stress relaxation test, while the textures reflected the final effect.

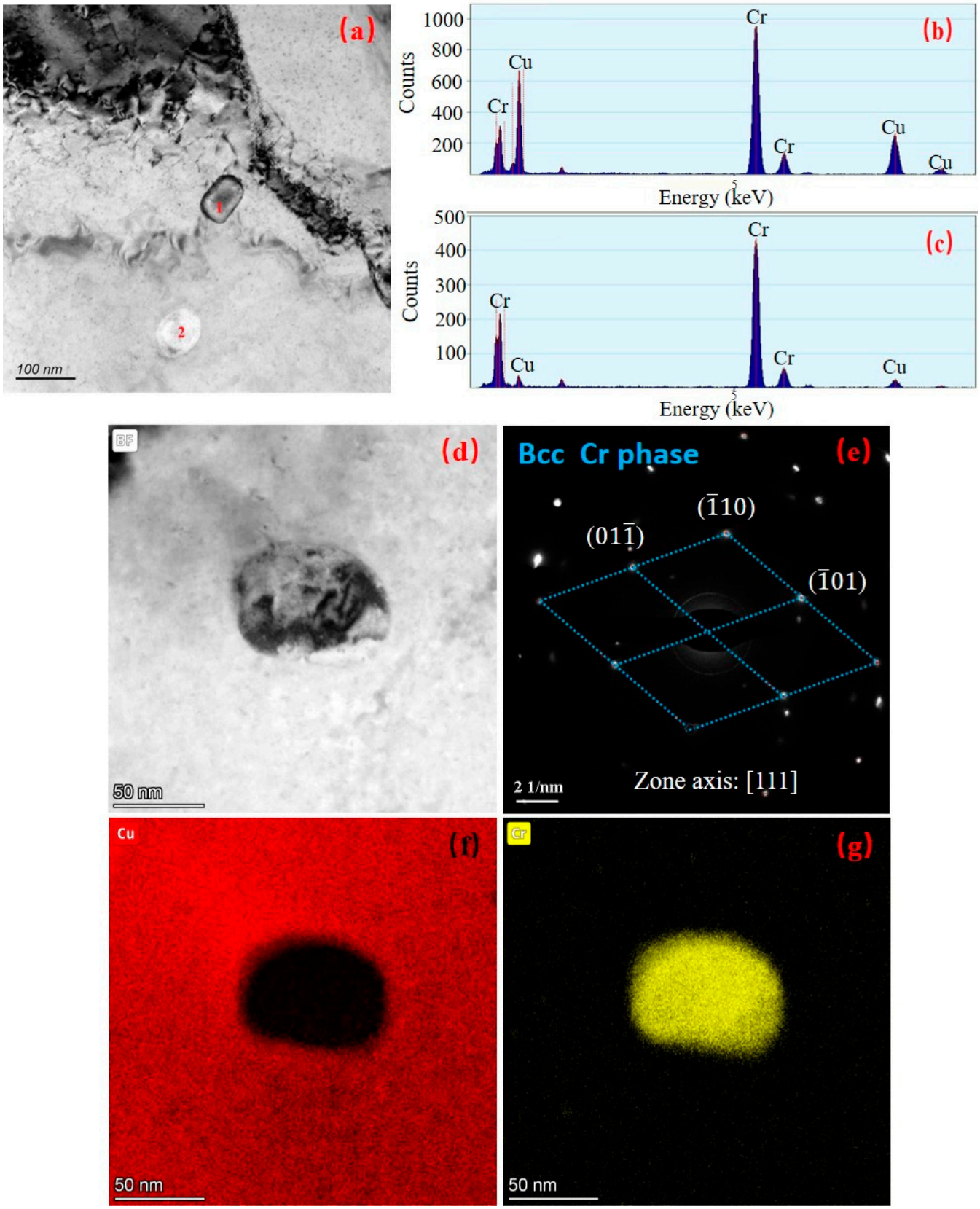


Figure 4. (**a**) BF–TEM image of the Cr-rich precipitates and (**b**,**c**) corresponding EDS point analyses; (**d**) BF–TEM image of the representative Cr phase (**e**) with corresponding SAD analysis and (**f**,**g**) EDS surface analyses.

3.2. Effect of Calefaction and Stress Relaxation on Grain Boundaries

Figure 5 shows the proportion and the variation in GBs in different states. The proportion of 0–5° LAGBs (green line) was as high as 50–57% for all the states, and a higher content of LAGBs indicated a higher dislocation density. The proportion of 5–15° medium-angle GBs was about 26–29%, and the proportion of 15–65° high-angle grain boundaries (HAGBs) was approximately 16–23% for all the states. Compared to the cold-rolled state, the proportion of GBs for both aging and heated states were altered because of calefaction. Compared to the heated state, the content of GBs in the relaxed state changed due to stress. As can be seen from Figure 5, the proportion of LAGBs decreases, while that of the medium-angle GBs changes slightly, and that of the HAGBs increases, under the influence of calefaction [34]. The proportion of LAGBs increases while the content of HAGBs decreases after stress relaxation.

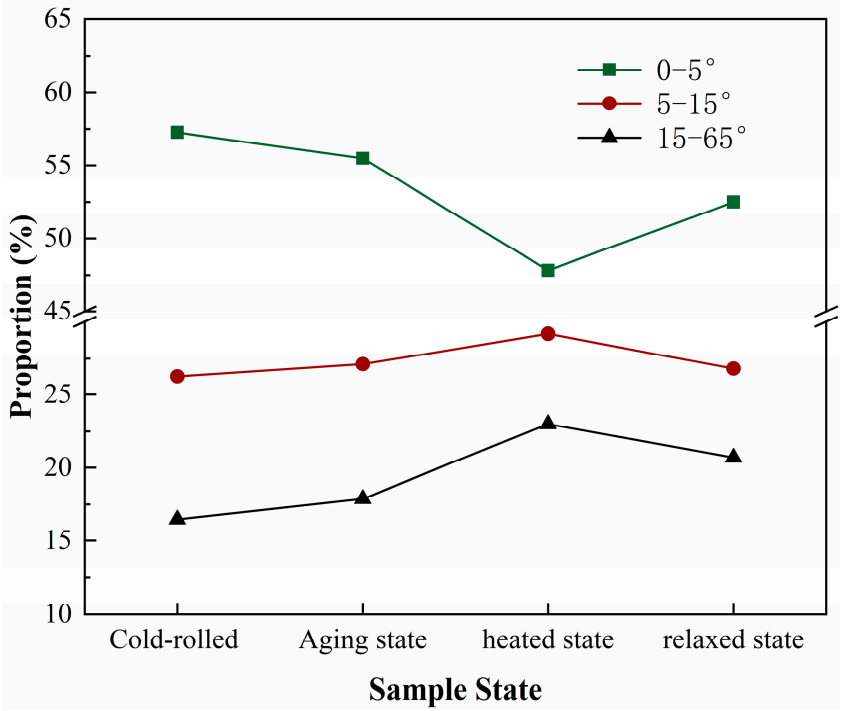


Figure 5. The proportion of different types of GBs in different states.

The content of LAGBs rose with the increasing deformation ratio [35]. Figure 6 shows the TEM morphologies of the Cu–Cr–Ni alloy in the aging state. A large number of sub-grains and dislocation interaction structures such as dislocation walls, dislocation cells, and dislocation entanglements are clearly observed, which correspond to the high-content LAGBs in Figure 5. Theoretically, the dislocation interaction structures can effectively impede the movement of dislocations through deformation strengthening [36]. However, dislocations are more likely to move when subjected to calefaction. As shown in Figure 5, the calefaction leads to a proportion decrease in LAGBs. It has been reported that the sliding motion of dislocation interaction structures reduces the stress relaxation resistance [37]. In the present study, the percentage of LAGBs increased after stress relaxation. The elastic deformation was transformed into plastic deformation during stress relaxation. During this process, massive dislocations slipped up, which led to an increase in the proportion of small-angle GBs. Relevant studies have shown that the material will generate more dislocations and increased LAGBs during deformation [38–40]. Therefore, the variation in LAGBs content proves that the nature of stress relaxation is related to dislocation motion. And calefaction can reduce the content of LAGBs, which deteriorates stress relaxation resistance.

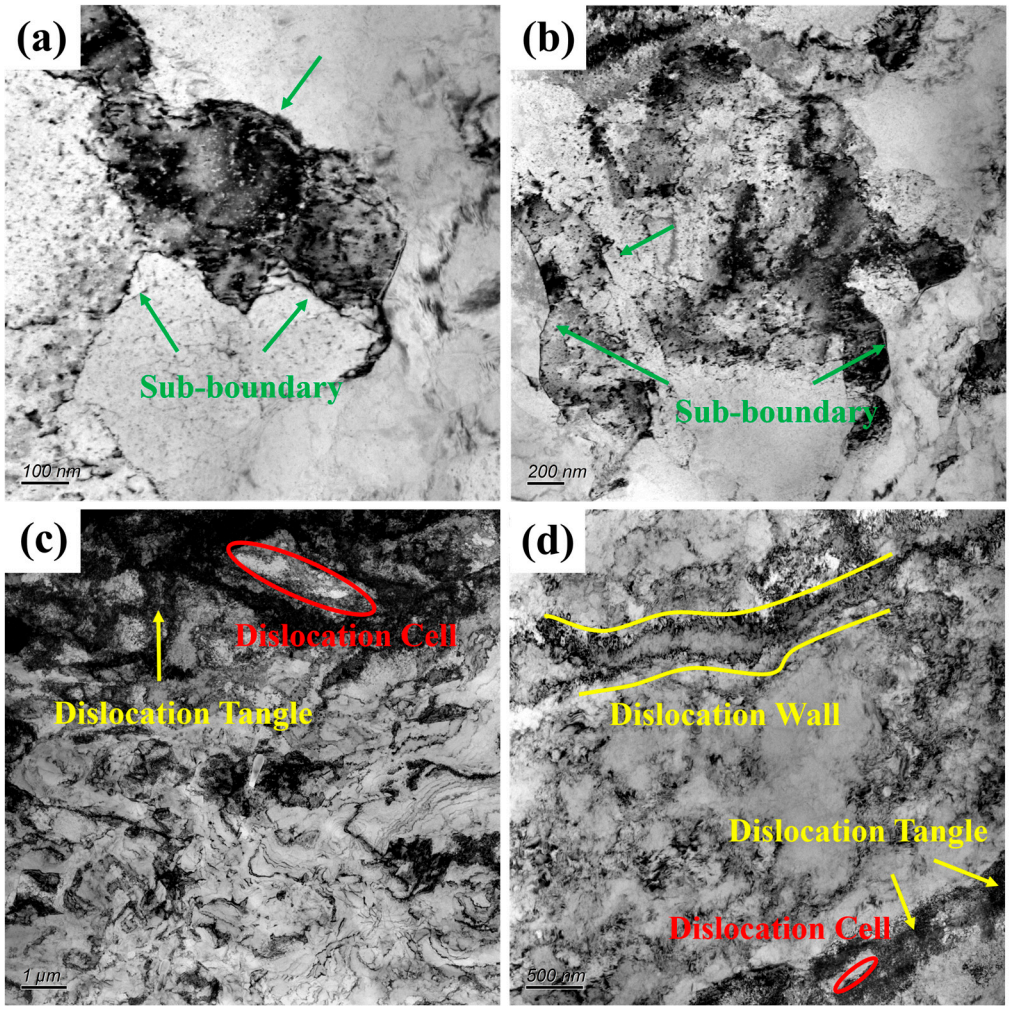


Figure 6. TEM investigations of the Cu–Cr–Ni alloy in aging state. (**a**,**b**) images of sub-grains; (**c**,**d**) morphologies of dislocations.

3.3. Effect of Calefaction and Stress Relaxation on Fiber Texture

When polycrystal is compressed or stretched, the rotation of the crystal will induce the formation of fiber textures [41,42]. Figure 7 shows the inverse pole figure (IPF) of the Cu–Cr–Ni alloy in different states in RD direction. From Figure 7a, the strength of <111> reaches a maximum value of 6.71, which indicates that the alloy obtains a preferred orientation (RD//<111>) after cold rolling with a large deformation. In Figure 7b, the strength of <111> decreases to 5.79, indicating that a short calefaction can cause a slight shift of the preferred orientation. Figure 7c shows that the preferred orientation of the heated state changes significantly after calefaction for a long time, shifting from <111> to <113>. The textures of the relaxed state are shown in Figure 7d, where it is found that the strength around <111> increases significantly, and the strength of <001> increases slightly. After stress relaxation, the preferred orientation shifts from <113> to <111> and <001>, indicating that the stress relaxation can significantly change the preferred orientation of the heated state.

In summary, the calefaction made the preferred orientation of the cold-rolled state deviate from <111>, but the preferred orientation re-approached the <111> direction after stress relaxation. The changes in fiber textures caused by calefaction or stress relaxation are shown in Figure 8. Cold-drawn Cu wire had bicomponent fiber textures of <111> and <001>, while the volume fraction of <111>-oriented grains increased during the deformation process [43,44]. The change in fiber textures after stress relaxation was consistent with cold

rolling, and the final result tended to RD//<111>. The results thus verify that the essence of stress relaxation is the transition from elasticity to plasticity.

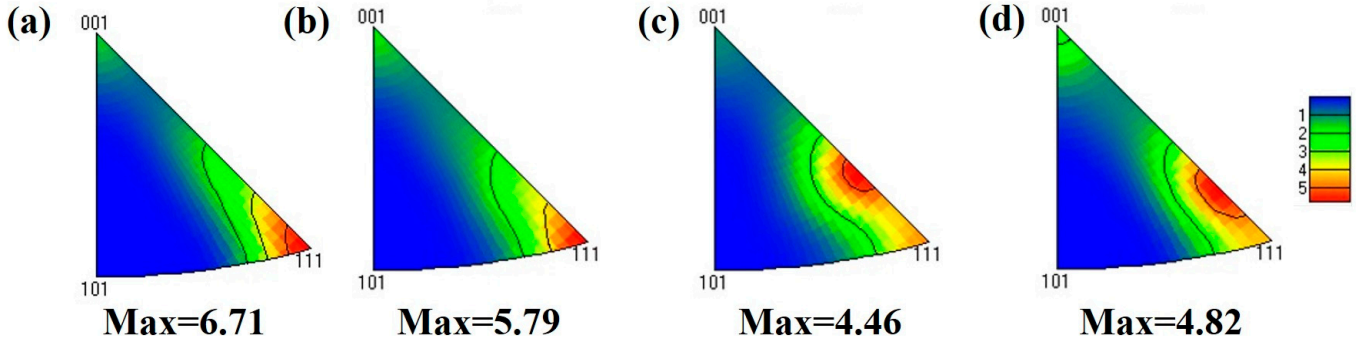


Figure 7. The IPF maps of Cu–Cr–Ni alloy in different states in RD direction: (**a**) cold-rolled state; (**b**) aging state; (**c**) heated state; (**d**) relaxed state.

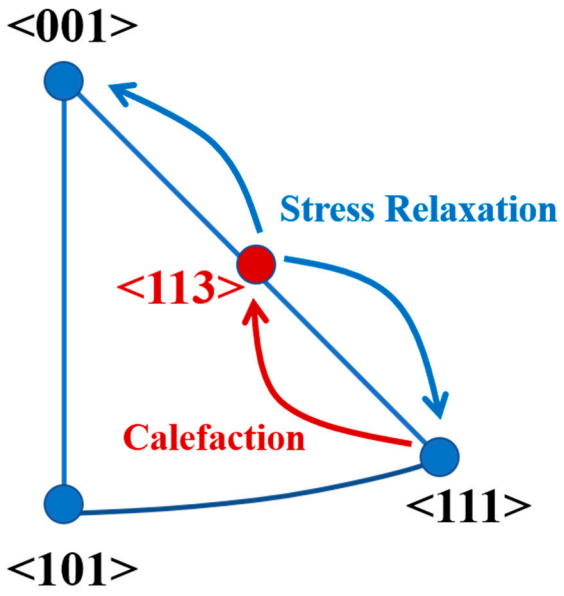


Figure 8. The changes in fiber texture after calefaction or stress relaxation.

3.4. Effect of Calefaction and Stress Relaxation on Plate Texture

Figure 9a–d show the orientation distribution function (ODF) of the Cu–Cr–Ni alloy in different states. It can be seen that the alloy had a Brass texture at 0° ODF, a strong Copper texture and a weak Brass texture at 45° ODF, and a S texture at 65° ODF. The plate textures in Figure 9 are consistent with the typical textures of rolled Cu alloys. The types of plate texture did not change after calefaction or stress relaxation, but the intensity of the Brass, Copper, and S textures did change, indicating that there was a transformation process between the plate textures.

Figure 10 shows the distribution of the Copper, S, and Brass textures in different states and the distribution of the Schmidt Factor (SF) on the (111) <−110> slip surface. From Figure 10a–d, it can be seen that the proportions of Copper and S textures are higher, but the proportion of Brass textures is lower. The insets show the unit cell corresponding to each type of texture. Comparing the texture and SF distributions, it can be found that different textures correspond to different SF values. Combining the statistics of different textures with their corresponding SF values, the SF values of the Copper, S, and Brass textures are 0.31–0.37, 0.41–0.47, and 0.41–0.46, respectively. We counted the twelve slip systems composed of {111} and [110], and all the statistical data were the same as (111) <−110> slip surfaces.

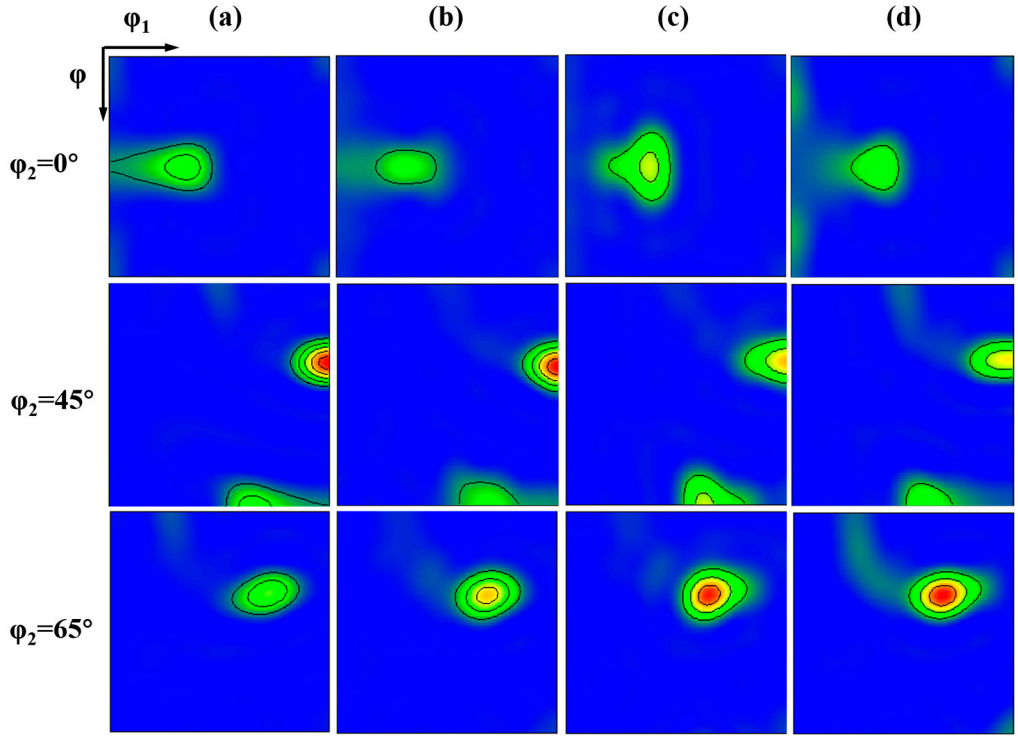


Figure 9. The ODF at 0°, 45°, and 65° of Cu–Cr–Ni alloy in different states: (**a**) cold-rolled state; (**b**) aging state; (**c**) heated state; (**d**) relaxed state.

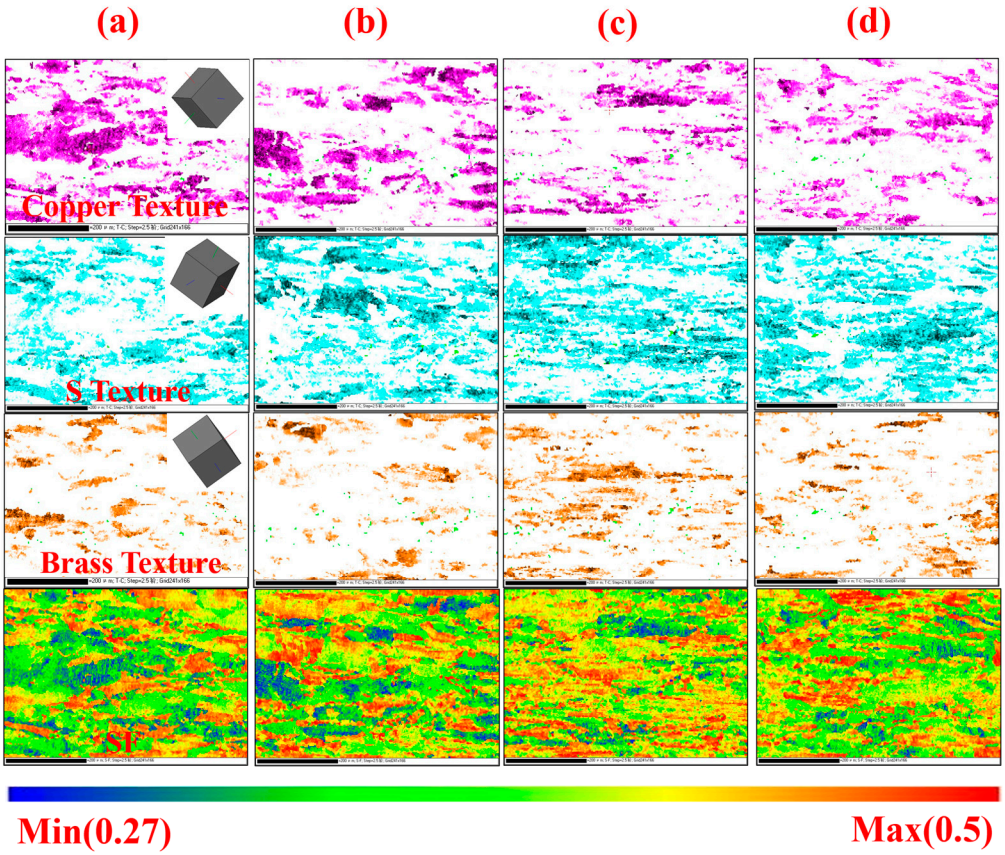


Figure 10. The distributions of textures and SF of Cu–Cr–Ni alloy in different states: (**a**) cold-rolled state; (**b**) aging state; (**c**) heated state; (**d**) relaxed state. The scale bar is 200 μm.

Figure 11 shows the variation tendency of SF values of the Cu–Cr–Ni alloy in different states. It can be seen that the SF in cold-rolled state exhibited a double-peak distribution. One peak with hard orientation was around 0.34 and the other peak with soft orientation was around 0.45. The change from cold-rolled state (black curve) to heated state (green curve) was influenced by calefaction. The textures (SF = 0.275–0.376) decreased significantly, while the textures (SF = 0.376–0.465) increased significantly after the calefaction. The transformation of SF indicated that the material had undergone a process from hard to soft orientation. The aging state (red curve) was also in accordance with the transition law of calefaction. It was not a coincidence that the SF curves of the cold-rolled state, aging state, and heated state intersected at 0.367. The turning point from hard orientation to soft orientation was SF = 0.367 under the calefaction. The calefaction led to an increase in soft orientation, so the crystals were more susceptible to plastic deformation. Soft orientation can accelerate the stress relaxation process and shorten the service life. The change from the heated state to the relaxed state was influenced by stress relaxation. The SF value of texture between 0.394 and 0.475 decreased, and the SF value between 0.315 and 0.394 increased. Stress relaxation transformed the soft orientation into the hard orientation.

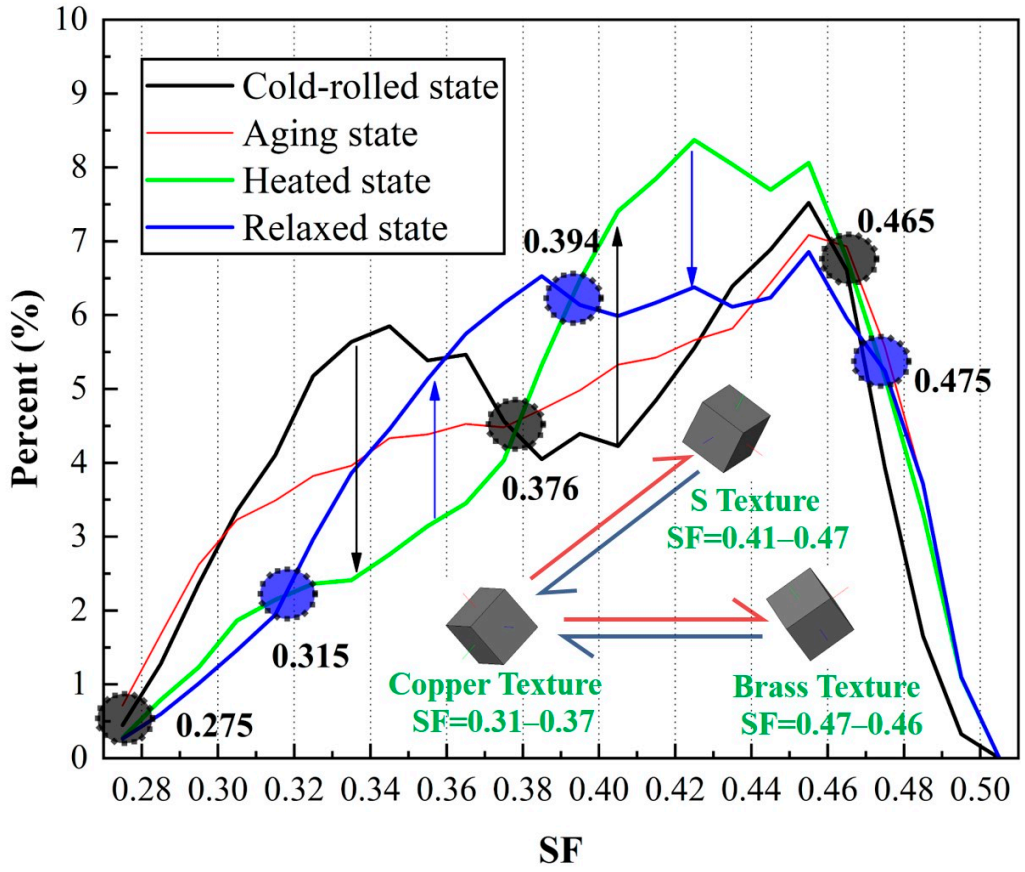


Figure 11. The variation tendency of SF of Cu–Cr–Ni alloy in different states and the transformation of plate textures.

The variation in SF was combined with the textures. The SF of the plate textures (Copper, S, Brass) was included in the change range of the SF of calefaction or stress relaxation. The ODF map shows that Copper, S, and Brass textures are strong textures. During the whole experiment, the types of texture did not change, but the intensity varied. The changes in SF indicate a transformation of textures from hard (Copper texture) to soft orientation (S and Brass texture), while the stress relaxation led to a transition from soft to hard orientation. The reduction in SF after stress relaxation was consistent with the study results of stretching, which indicates that the essence of stress relaxation is the same as that

of stretching, and both are related to the process of transformation from elastic deformation to plastic deformation [45].

4. Conclusions

1. The effect of stress relaxation on the GBs is opposite to that of the calefaction. Calefaction can reduce the proportion of LAGBs, leading to a decrease in stress relaxation resistance, which is related to the dislocation motion.
2. The Cu–Cr–Ni alloy forms a preferred <111>-orientated texture after cold rolling. However, the preferred orientation tilts toward the <113> direction due to the calefaction, while shifting toward the <111> and <100> directions after stress relaxation.
3. The Cu–Cr–Ni alloy is composed of Brass, S, and Copper textures regardless of the state. After calefaction or stress relaxation, the texture type does not change but the proportion varies. The SF transforms from hard to soft orientation under calefaction, and from soft to hard orientation when subjected to stress relaxation.
4. The reduction in SF after the stress relaxation is consistent with the stretching results, indicating that stress relaxation is a transformation process that transitions from elastic to plastic deformation.

Author Contributions: H.L.: Conceptualization, Funding Acquisition, Writing—Review and Editing. G.W.: Formal Analysis, Investigation, Writing—Original Draft. K.S.: Conceptualization, Funding Acquisition. Y.H.: Investigation, Writing—Original Draft. Y.L.: Supervision, Investigation. T.H.: Conceptualization, Writing—Review and Editing. All authors have read and agreed to the published version of the manuscript.

Funding: The authors gratefully acknowledge the financial support received from the Henan Province Young Talent Lifting Engineering Project (No. 2021HYTP018), the National Programs for Science and Technology Development of Henan Province (No. 222102230001) and the Zhongyuan Scholars Workstation Project (No. 224400510025), the National Natural Science Foundation of China (Nos. 52071133 and 51904090), the China Engineering Science and Technology Development Strategy Henan Research Institute Strategic Consulting Research Project (No. 2021HENZDA02).

Data Availability Statement: The data presented in this study are available on request from the corresponding author. The data are not publicly available due to privacy.

Acknowledgments: The authors would like to thank Xiaowen Peng and Shijun Liang for the supervision and investigation during the preparation of the manuscript.

Conflicts of Interest: The authors declare that they have no known competing financial interests or personal relationships that could have appeared to influence the work reported in this paper.

References

1. Weber, M.; Helm, D. Prediction of the behaviour of copper alloy components under complex loadings by electro-thermomechanical coupled simulations. *Mater. Sci. Technol.* **2018**, *36*, 899–905. [CrossRef]
2. Liao, K.C.; Chang, C.C. Relaxation investigation on durability for terminals of CPU socket connectors. *Mater. Des.* **2009**, *30*, 252–255. [CrossRef]
3. Sharififar, M.; Akbari Mousavi, S.A.A. Tensile deformation and fracture behavior of CuZn5 brass alloy at high temperature. *Mater. Sci. Eng. A* **2014**, *594*, 118–124. [CrossRef]
4. Chen, K.J. Novel application research on critical high-temperature deformation of low-lead brass alloy. *Metals* **2020**, *10*, 722. [CrossRef]
5. Yang, X.S.; Wang, Y.J.; Wang, G.Y.; Zhai, H.R.; Dai, L.H.; Zhang, T.Y. Time, stress, and temperature-dependent deformation in nanostructured copper: Stress relaxation tests and simulations. *Acta Mater.* **2016**, *108*, 252–263. [CrossRef]
6. Lyu, F.; Li, Y.; Shi, Z.S.; Huang, X.; Zeng, Y.S.; Lin, J.G. Stress and temperature dependence of stress relaxation ageing behaviour of an Al-Zn-Mg alloy. *Mater. Sci. Eng. A* **2020**, *773*, 138859. [CrossRef]
7. Peng, H.L.; Hou, Z.Q.; Chen, X.; Li, T.L.; Luo, J.F.; Li, X.F. Effect of temperature and cyclic loading on stress relaxation behavior of Ti-6Al-4V titanium alloy. *Mater. Sci. Eng. A* **2021**, *824*, 141789. [CrossRef]
8. Siska, F.; Stratil, L.; Smid, M.; Luptakova, N.; Zalezak, T.; Bartkova, D. Deformation and fracture behavior of the P91 martensitic steel at high temperatures. *Mater. Sci. Eng. A* **2016**, *672*, 1–6. [CrossRef]
9. Sun, Y.Q.; Peng, L.J.; Huang, G.J.; Feng, X.; Xie, H.F.; Mi, X.J.; Liu, X.H. Effect of Mg on the stress relaxation resistance of Cu–Cr alloys. *Mater. Sci. Eng. A* **2021**, *799*, 140144. [CrossRef]

10. Shah, N.S.; Sunil, S.; Sarkar, A. High temperature uniaxial compression and stress–relaxation behavior of india-specific RAFM Steel. *Metall. Mater. Trans. A* **2018**, *49*, 2644–2653. [CrossRef]
11. Cheng, C.; Feng, Y.; Chen, Z.Y.; Li, H.E.; Wang, X.; Wang, Q.J. Effect of annealing temperature on microstructure, texture and tensile properties of TA32 sheet. *Mater. Sci. Eng. A* **2021**, *826*, 141971. [CrossRef]
12. Ji, Y.T.; Suo, H.L.; Liu, J.; Ma, L.; Liu, M.; Shaheen, K.; Wang, Y.; Zhang, Z.L.; Wang, Q.L. Effect of stress-relief annealing on rolled texture of nickel-based alloys. *J. Alloys Compd.* **2022**, *903*, 163970. [CrossRef]
13. Ban, Y.J.; Zhang, Y.; Jia, Y.L.; Tian, B.H.; Volinsky, A.A.; Zhang, X.H.; Zhang, Q.F.; Geng, Y.F.; Liu, Y.; Li, X. Effects of Cr addition on the constitutive equation and precipitated phases of copper alloy during hot deformation. *Mater. Des.* **2020**, *191*, 108613. [CrossRef]
14. Shen, F.H.; Zhou, Z.R.; Li, W.F.; Sun, Z.Z.; Tian, J.; Xie, C.X.; Guo, J.W.; Liao, Z.L.; Yi, D.Q.; Zhang, J.Y.; et al. Micro-mechanism of texture evolution during isochronal annealing of as-annealed hot rolled Al-Cu-Mg sheet. *Mater. Des.* **2019**, *165*, 107575. [CrossRef]
15. Gao, X.; Wu, H.B.; Liu, M.; Zhang, Y.X.; Gao, F.; Zhou, X.D. Texture and special grain boundary distribution of C71500 copper-nickel alloy tubes at different annealing temperatures. *J. Mater. Eng. Perform.* **2021**, *30*, 2365–2373. [CrossRef]
16. Liu, Y.Z.; Sun, J.H.; Zhou, L.Y.; Tu, Y.G.; Xing, F.; Guo, Y.C.; Tong, Q. Experiment investigation of deep-drawing sheet texture evolution. *J. Mater. Process. Technol.* **2003**, *140*, 509–513. [CrossRef]
17. Chen, W.; Chen, M.H.; Feng, S.H.; Jin, X.J. Effect of crystallographic texture on the anisotropic tensile behavior of aluminum foil and its industrial application. *J. Mater. Eng. Perform.* **2021**, *31*, 1306–1316. [CrossRef]
18. Yang, F.; Dong, L.M.; Cai, L.; Wang, L.F.; Xie, Z.H.; Fang, F. Effect of cold drawing strain on the microstructure, mechanical properties and electrical conductivity of low-oxygen copper wires. *Mater. Sci. Eng. A* **2021**, *818*, 141348. [CrossRef]
19. Aghamiri, S.M.S.; Oono, N.; Ukai, S.; Kasada, R.; Noto, H.; Hishinuma, Y.; Muroga, T. Brass-texture induced grain structure evolution in room temperature rolled ODS copper. *Mater. Sci. Eng. A* **2019**, *749*, 118–128. [CrossRef]
20. Wei, H.; Chen, Y.L.; Zhao, Y.N.; Yu, W.; Su, L.; Tang, D. Correlation mechanism of grain orientation/microstructure and mechanical properties of Cu-Ni-Si-Co alloy. *Mater. Sci. Eng. A* **2021**, *814*, 141239. [CrossRef]
21. Wang, C.S.; Fu, H.D.; Xie, J.X. Dynamic recrystallization behavior and microstructure evolution of high-performance Cu-3.28Ni-0.6Si-0.22Zn-0.11Cr-0.04P during hot compression. *Rare Met.* **2021**, *40*, 156–167. [CrossRef]
22. Geng, Y.F.; Ban, Y.J.; Li, X.; Zhang, Y.; Jia, Y.L.; Tian, B.H.; Zhou, M.; Liu, Y.; Volinsky, A.A.; Song, K.X.; et al. Excellent mechanical properties and high electrical conductivity of Cu-Co-Si-Ti alloy due to multiple strengthening. *Mater. Sci. Eng. A* **2021**, *821*, 141639. [CrossRef]
23. Liu, W.J.; Chen, X.; Ahmad, T.; Zhou, C.Y.; Xiao, X.P.; Wang, H.; Yang, B. Microstructures and mechanical properties of Cu-Ti alloys with ultrahigh strength and high ductility by thermo-mechanical treatment. *Mater. Sci. Eng. A* **2022**, *835*, 142672. [CrossRef]
24. Zhang, Y.Y.; Tang, M.X.; E, J.C.; Zhong, Z.Y.; Luo, S.N. Texture evolution of Cu nanopowder under uniaxial compression. *Materialia* **2018**, *1*, 236–243. [CrossRef]
25. Yang, J.Z.; Bu, K.; Song, K.X.; Zhou, Y.J.; Huang, T.; Niu, L.Y.; Guo, H.W.; Du, Y.B.; Kang, J.W. Influence of low-temperature annealing temperature on the evolution of the microstructure and mechanical properties of Cu-Cr-Ti-Si alloy strips. *Mater. Sci. Eng. A* **2020**, *798*, 140120. [CrossRef]
26. Watanabe, C.; Monzen, R.; Tazaki, K. Mechanical properties of Cu-Cr system alloys with and without Zr and Ag. *J. Mater. Sci.* **2008**, *43*, 813–819. [CrossRef]
27. Li, P.F.; Zou, M.Q.; Song, C.Y.; Qi, L.; Guan, R.G. Research on the stress relaxation behaviour of Cu-0.23Cr-0.08Ag alloy. *Mater. Sci. Technol.* **2021**, *37*, 458–466. [CrossRef]
28. Buchhagen, P.; Riehemann, W. Stress relaxation in precipitation-hardenable alloys. *J. Alloys Compd.* **1994**, *211–212*, 509–513. [CrossRef]
29. Yang, Y.L.; Zhan, L.H.; Liu, C.H.; Wang, X.; Wang, Q.; Tang, Z.M.; Tang, Z.M.; Li, G.P.; Huang, M.H.; Hu, Z.G. Stress-relaxation ageing behavior and microstructural evolution under varying initial stresses in an Al-Cu alloy: Experiments and modeling. *Int. J. Plast.* **2020**, *127*, 102646. [CrossRef]
30. Wang, G.J.; Liu, H.T.; Song, K.X.; Zhou, Y.J.; Cheng, C.; Guo, H.W.; Guo, Y.G.; Tian, J. Aging process and strengthening mechanism of Cu–Cr–Ni alloy with superior stress relaxation resistance. *J Mater. Res. Technol.* **2022**, *19*, 3579–3591. [CrossRef]
31. *GB/T 34505-2017*; Copper and Copper Alloy Materials—Tensile Testing at Room Temperature. National Standards of the People's Republic of China: Beijing, China, 2017.
32. Geng, Y.F.; Li, X.; Zhou, H.L.; Zhang, Y.; Jia, Y.L.; Tian, B.H.; Liu, Y.; Volinsky, A.A.; Zhang, X.H.; Song, K.X.; et al. Effect of Ti addition on microstructure evolution and precipitation in Cu-Co-Si alloy during hot deformation. *J. Alloys Compd.* **2020**, *821*, 153518. [CrossRef]
33. Zhang, Y.L.; Wang, H.; Sun, H.Y.; Chen, G. Effects of annealing temperature on the microstructure, textures and tensile properties of cold-rolled Fe-13Cr-4Al alloys with different Nb contents. *Mater. Sci. Eng. A* **2020**, *798*, 140236. [CrossRef]
34. Zhang, P.; Wang, H.; Yao, S.J.; Wang, C.J.; Zhu, Q.; Chen, G. Effect of annealing on the microstructure, texture and tensile deformation properties of Cu-3 wt%Ag-0.5 wt%Zr thin sheets rolled at room and cryogenic temperature. *Met. Mater. Int.* **2021**, *27*, 392–402. [CrossRef]
35. Tong, L.B.; Zhang, J.B.; Zhang, Q.X.; Jiang, Z.H.; Xu, C.; Kamado, S.; Zhang, D.P.; Meng, J.; Cheng, L.R.; Zhang, H.J. Effect of warm rolling on the microstructure, texture and mechanical properties of extruded Mg-Zn-Ca-Ce/La alloy. *Mater. Charact.* **2016**, *115*, 1–7. [CrossRef]

36. Dasharath, S.M.; Mula, S. Microstructural evolution and mechanical properties of low SFE Cu-Al alloys processed by cryorolling followed by short-annealing. *Mater. Des.* **2016**, *99*, 552–564. [CrossRef]
37. Xiao, X.P.; Xu, H.; Huang, J.; Wang, J.F.; Zhang, J.B. Stress relaxation properties and microscopic deformation structure in bending of the C7025 and C7035 alloy. *Crystals* **2018**, *8*, 324. [CrossRef]
38. Kumar, S. Evaluation of strain hardening during uniaxial tensile loading followed by stress relaxation and reloading. *Metall. Mater. Trans. A* **2022**, *53*, 1336–1344. [CrossRef]
39. Ifergane, S.; Barkay, Z.; Beeri, O.; Eliaz, N. Study of fracture evolution in copper sheets by in situ tensile test and EBSD analysis. *J. Mater. Sci.* **2010**, *45*, 6345–6352. [CrossRef]
40. Youngdahl, C.J.; Weertman, J.R.; Hugo, R.C.; Kung, H.H. Deformation behavior in nanocrystalline copper. *Scripta Mater.* **2001**, *44*, 1475–1478. [CrossRef]
41. Liu, S.C.; Gao, Y.; Lin, Z.L.; Guo, S.S.; Zhang, X.B.; Yin, X.J. Microstructure and properties after deformation and aging process of A286 superalloy. *Rare Met.* **2019**, *38*, 864–870. [CrossRef]
42. Ripoll, M.R.; Očenášek, J. Microstructure and texture evolution during the drawing of tungsten wires. *Eng. Fract. Mech.* **2009**, *76*, 1485–1499. [CrossRef]
43. Popova, E.N.; Popov, V.V.; Romanov, E.P.; Hlebova, N.E.; Shikov, A.K. Effect of deformation and annealing on texture parameters of composite Cu-Nb wire. *Scripta Mater.* **2004**, *51*, 727–731. [CrossRef]
44. Narayanan, K.R.; Sridhar, I.; Subbiah, S. Experimental and numerical investigations of the texture evolution in copper wire drawing. *Appl. Phys. A* **2012**, *107*, 485–495. [CrossRef]
45. Zhang, W.J.; Lu, J.X.; Wang, J.; Sang, L.J.; Ma, J.Y.; Zhang, Y.F.; Zhang, Z. In-situ EBSD study of deformation behavior of Inconel 740H alloy at high-temperature tensile loading. *J. Alloys Compd.* **2020**, *820*, 153424. [CrossRef]

Disclaimer/Publisher's Note: The statements, opinions and data contained in all publications are solely those of the individual author(s) and contributor(s) and not of MDPI and/or the editor(s). MDPI and/or the editor(s) disclaim responsibility for any injury to people or property resulting from any ideas, methods, instructions or products referred to in the content.